Examination of plasma-wall interactions in Hall effect thrusters by means of calibrated thermal imaging

S. Mazouffre[a] and K. Dannenmayer
ICARE, CNRS, 1C Avenue de la Recherche Scientifique, 45071 Orléans, France

J. Pérez-Luna
LAPLACE, Paul Sabatier University, 118 Route de Narbonne, 31062 Toulouse Cedex 9, France

(Received 2 February 2007; accepted 8 June 2007; published online 25 July 2007)

A semiempirical time-dependent thermal model of Hall effect thrusters was developed to compute evolution of the thruster channel wall temperature during a transient regime. The model accounts for heat conduction through dielectric walls and radiative transfer as the channel is considered as a thermal enclosure. The graybody view factors are experimentally determined during the cooling period that follows a power shutdown. The model permits the assessment of the amount of power delivered to walls by fitting calculated temperature profiles to experimental profiles obtained by means of calibrated infrared imaging. Plasma-surface interactions are examined in this contribution for three types of thrusters, namely, SPT100-ML, PPS®1350-G, and the 5-kW-class PPSX000-ML. The electrical input power range that is probed stretches out from 500 W to 5 kW. The energy flux passed to the discharge chamber dielectric walls varies between 0.1 and 2 W/cm^2. The overall amount of power delivered to the external and internal walls is found to vary linearly with the applied power. It is in favor of an energy loss mechanism driven by ion bombardment. A departure from the linear trend is observed at high discharge voltage. Production of multiply charged ion species could be an explanation. The impact of thruster design and wall material on power losses inside the thruster channel is also investigated from both a technological and a physics standpoint.
 [DOI: 10.1063/1.2757716]

I. INTRODUCTION

Hall effect thrusters (HETs) are advanced electric propulsion devices for spacecrafts.[1,2] The basic physics of a HET consists of a magnetic barrier in a low pressure dc discharge generated between an external hollow cathode and an anode located at the upstream end of a coaxial annular dielectric channel that confines the discharge.[3] Along their path, electrons encounter a region of high resistivity in the vicinity of the channel exhaust due to a strong applied radial magnetic field and they become trapped. The magnetic field is chosen strong enough to make the electron Larmor radius much smaller than the discharge chamber length but weak enough not to affect ion trajectories. The electric potential drop is, therefore, mostly concentrated in the final section of the channel. The corresponding induced local axial electric field has two main effects. First, it drives a high electron azimuthal drift—the so-called Hall current—that is responsible for the efficient ionization of the supplied gas. Second, it accelerates out of the channel the created ions, which generates thrust. While the specific design of a HET results in an efficient low thrust, high specific impulse device suitable for various space applications, physical phenomena and processes at work in such a device are still misunderstood, especially electron transport and plasma-wall interactions.

Plasma-surface interactions inside the channel govern to a large extent the thruster thermal state, plasma properties, as well as wear of walls. As a consequence, plasma-surface interactions have a drastic impact upon the operation envelope, the overall performance level, and the thruster lifetime. One way to gain insights into plasma-surface interactions is to monitor the temperature of thruster components, especially dielectric channel walls, during thruster firing. The thermal behavior of HETs in steady state has been extensively examined over the last few years either by means of thermocouples embedded in the thruster structure[4] or more recently by means of infrared thermal imaging.[5] Such studies are of interest on a technological standpoint as they allow to design the heat release system to warrant a broad operation domain. On a more fundamental viewpoint, these studies allow a better understanding of the effect of thruster design, geometry, input power, and channel wall material upon energy loss mechanisms at work inside the discharge chamber. Nevertheless, this approach does not provide with quantitative data about power passed to walls by way of ion and electron bombardment.

In this contribution, we first describe then apply a method that permits us to assess the energy flux passed to the channel walls by the plasma. The goal is achieved, thanks to a subtle combination of infrared thermal imaging with computational simulations. A semiempirical time-dependent thermal model of Hall effect thrusters was developed to compute evolution of the thruster channel wall temperature during a transient regime. The model allows us to determine the amount of power delivered to walls by fitting calculated temperature profiles to experimental profiles. In this work plasma-surface interactions are examined for three types of thrusters, namely, SPT100-ML, PPS®1350-G, and the high

[a]Electronic mail: stephane.mazouffre@cnrs-orleans.fr

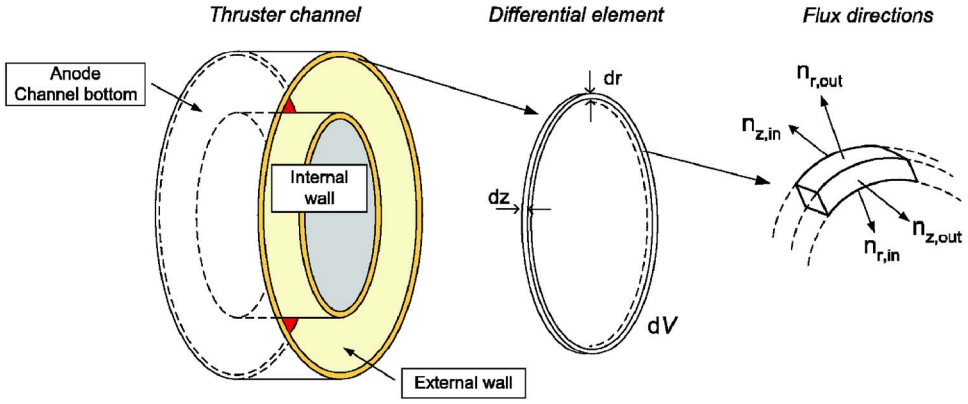

FIG. 1. Simplified drawing of all components that make up the channel of a Hall effect thruster: internal and external dielectric rings, bottom, and anode. The anode, which also acts as gas injector, is, in fact, placed on the rear ceramic disk (bottom). Also shown are the differential element and the flux direction considered in the model to establish the energy conservation equation for a channel wall element.

power PPSX000-ML. Hence, the power range that is probed stretches out from 500 W to 5 kW. In addition to studying the impact of thruster design and size on power losses inside the channel, the influence of gas flow, discharge voltage, and wall material is also investigated.

II. TIME-DEPENDENT THERMAL MODEL OF A HET

A. Energy conservation equation

As we are interested in examining plasma-surface interactions and related power losses inside the thruster discharge chamber, or channel, we need first to give a short overview of the channel geometry and properties. The channel is composed of two concentric cylinders of length l and thickness h and fabricated of nonconducting material, e.g., $BN-SiO_2$. It is closed on one side and open on the other side to let the plasma expands into a vacuum. The channel bottom is fabricated with ceramic. A ring-shape hollow anode, which also acts as gas injector, is located at the very back part of the channel. It may or not entirely cover the channel dielectric bottom, depending on the exact thruster architecture. The channel geometry is sketched in Fig. 1. For a SPT100-type thruster, usual dimensions are $l=25$ mm, $h=4.5$ mm, $r_{\text{ext}}=50$ mm, and $r_{\text{int}}=35$ mm, where r_{ext} and r_{int} are, respectively, the channel external and internal wall radii.

A time-dependent thermal model of a Hall effect thruster channel is naturally based on the energy conservation equation. As shown in previous works, the channel wall temperature does not vary much with the azimuthal angle.[6,7] Therefore, the first assumption is to consider the problem as axisymmetric. The differential element of interest is then the elementary ring shown in Fig. 1. The same equation applies for an element of the external wall and for an element of the internal wall. However, as we will see, boundary conditions for the two elements differ. Let T be the temperature of the elementary volume dV, E its energy, ρ its density, and ϕ_i the outgoing energy rates through the corresponding surfaces dS_i. The energy equation for the control volume dV reads

$$\rho\frac{dE}{dt}dV=-\sum_i \phi_i\cdot\mathbf{n}_i\,dS_i, \tag{1}$$

where t is the time.[8] The considered volume being motionless, the energy reduces to the enthalpy H, $dE=dH=c_p\,dT$, where c_p is the specific heat. Using the sign convention of Fig. 1, the energy conservation equation takes the form

$$\rho c_p\frac{\partial T}{\partial t}dV=-\phi_{r,\text{out}}\cdot\mathbf{n}_{r,\text{out}}dS_{r,\text{out}}-\phi_{r,\text{in}}\cdot\mathbf{n}_{r,\text{in}}dS_{r,\text{in}}-\phi_{z,\text{out}}\cdot\mathbf{n}_{z,\text{out}}dS_z-\phi_{z,\text{in}}\cdot\mathbf{n}_{z,\text{in}}dS_z, \tag{2}$$

where the subscripts *out* and *in* refer to the outer and inner sides of a channel wall element, respectively. The channel walls' thickness h is small in comparison with the internal and external channel wall radii. We can therefore consider that $dS_{r,\text{out}}\approx dS_{r,\text{in}}=dS_r$. Previous equation then takes the simpler form

$$\rho c_p\frac{\partial T}{\partial t}dV=-(\phi_{r,\text{out}}\cdot\mathbf{n}_{r,\text{out}}+\phi_{r,\text{in}}\cdot\mathbf{n}_{r,\text{in}})dS_r-(\phi_{z,\text{out}}\cdot\mathbf{n}_{z,\text{out}}+\phi_{z,\text{in}}\cdot\mathbf{n}_{z,\text{in}})dS_z. \tag{3}$$

At that point, one must list the different heat rates involved in energy transfer processes inside the channel of a Hall effect thruster and discuss their respective magnitude in order to be able to simplify the right-hand side (RHS) term in Eq. (3). Five cases must be envisaged here, each related to a specific physical mechanism. First, Hall effect thrusters operate in a rarefied environment and the plasma inside the channel is at a low pressure (typically 1 Pa). As a consequence convective heat flux can be neglected. Second, at high temperature and in the case of dielectric walls, the amount of power transferred along the z direction by heat conduction[9] is much less than the power lost by way of radiation.[10] Third, in radial direction, one must distinguish between two kinds of elements. For a bulk element, conductive heat transfer across the wall must be taken into account. For a boundary element, heat is exchanged, thanks to radiative processes. The exact mathematical description of the radiative heat flux ϕ_{rad} will be developed in Sec. II C. In short, ϕ_{rad} depends on T^4, and radiation exchange between surfaces is taken into account using geometric configuration factors. Fourth, energy exchanges at the edge of the channel walls are neglected in view of the small area into play ($\approx 2\pi rh$ as $r\gg h$). Fifth, plasma-surface interactions play a key role in energy exchange processes inside the channel; they are characterized here at a macroscopic level by the energy flux deposited onto a surface element q_p. As we will see later in the text, the magnitude of q_p will be inferred from direct comparison between numerical outcomes and experimental data.

Finally, neglecting convective effects, heat conduction in the z direction, and boundary effects, the energy conservation equation for a HET channel wall element reads

$$\rho c_p \frac{\partial T}{\partial t} dr = -(\phi_{r,\text{out}} \cdot \mathbf{n}_{r,\text{out}} + \phi_{r,\text{in}} \cdot \mathbf{n}_{r,\text{in}}), \tag{4}$$

with $dV = 2\pi dr dz$ and $dS_r = 2\pi r dz$. Note that this equation solely depends on the r direction even if the influence of the whole thruster structure is, in fact, hidden within configuration factors. In the next sections we address the problem of finding the solution to Eq. (4) and we describe two solving methods that both allow us to determine q_p.

B. A simple way to solve the problem

At thruster ignition, heat conduction dominates energy exchange processes in view of the low channel temperature. The energy conservation equation then reduces to Fourier's law of heat conduction and, at first sight, the channel wall can be considered as an infinitely thick plane plate.[6] However, this very simple model is solely valid for a short time period in the order of 10 s since the relation $h < \sqrt{\alpha t}$, where α is the thermal diffusivity, must be satisfied. At thruster ignition, due to outgassing phenomena the discharge current varies in time, meaning that plasma properties are not stationary, especially q_p, and Fourier's law cannot be solved. Therefore in most cases this model cannot be used right after ignition. Moreover, this rough model assumes that the wall can store an infinite amount of energy. As a consequence, when applying this approach for a long time period $\Delta t > h^2/\alpha$ during which q_p does not vary, the value of q_p obtained from a comparison between calculations and measurements is overestimated.

Instead of considering a wall of infinite thickness, a better assumption is to consider that the temperature gradient through the wall is always zero. This assumption seems reasonable in view of the relatively low ceramic wall thickness. Let us now consider heat transport mechanism during a very short period of time. At high temperatures, the radiation characteristic time scale is far smaller than the conduction characteristic time scale.[10] Heat conduction can then be canceled out. Under this assumption, the energy conservation equation can be written as

$$\rho c_p \frac{\partial T}{\partial t} dr = -\phi_{\text{rad}} + q_p - \phi_{\text{outside}}, \tag{5}$$

where ϕ_{outside} stands for the energy evacuated outward and q_p is the energy flux lost at the wall by the plasma (see Fig. 2). The last term only appears in the equation that concerns the external wall. Indeed, the internal ceramic wall does not evacuate power through its inner side since it radiates on itself (the existence of a magnetic coil is neglected in this picture). Equation (5) allows us to extract the value of q_p in an elegant manner when considering either a thruster shutoff stage or a hot ignition stage, i.e., starting from a warm thruster, far from thermal equilibrium. Indeed, one can easily demonstrate that q_p can be expressed as

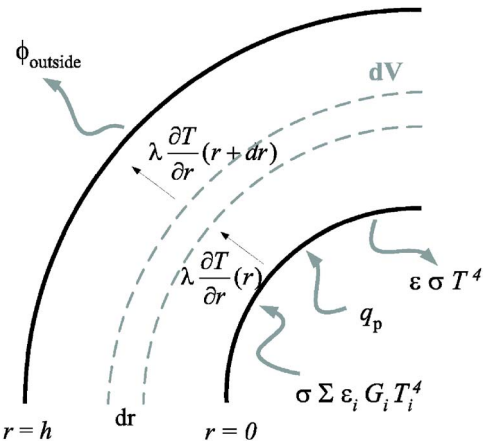

FIG. 2. Energy balance for the external channel wall used in the semiempirical time-dependent thermal model. The internal wall, on the contrary, is assumed to be adiabatic and $\phi_{\text{outside}} = 0$.

$$q_p = \rho c_p h \left(\left.\frac{dT}{dt}\right|_{t_0^-} - \left.\frac{dT}{dt}\right|_{t_0^+} \right), \tag{6}$$

where t_0^- and t_0^+ are the very moments just before and just after a power shutdown.[11]

Thus the energy flux deposited by the plasma onto a wall element is given by the slope difference of the temperature curves before and after the shutdown. The same technique applies for a hot ignition stage; however, terms in the RHS of Eq. (6) must be inverted. This method, the so-called "go and stop" approach, is attractive as it is perfectly adapted to the infrared imaging technique.[11] Moreover, this approach can be applied to any operating conditions. Nevertheless, this easy way of extracting data has some drawbacks. First, shutoff and ignition of the thruster can be at the origin of phenomena such as wall outgassing and ejection of matter from surfaces that are not taken into account. Second, slopes can only be determined with a good accuracy if a high temporal resolution is set, which necessitates a high data storage capacity. Notice that under identical thruster operating conditions the slopes are found to slightly vary from one measurement to another. Third, this method requires a dedicated operation on the thruster, i.e., shutdown or ignition. To sum up, as shown in a preceding work with the PPSX000-ML thruster,[11] this method, though simple and fast, solely permits us to determine rough values of q_p and to observe trends. For all aforementioned reasons, it appears of great interest to develop a more elaborated method to solve the thruster channel energy conservation equation, a method which, in addition, would permit us to accurately estimate q_p at any moment without modifying thruster working parameters.

C. The semiempirical approach

As a next step in building toward a more complex treatment that can fulfill all requirements, the channel will now be taken as a whole and we will develop a simple, though reliable, method that allows us to reproduce the observed temperature fields and ultimately to determine q_p. Instead of performing full calculation of energy transfer between all thruster components, a complex and cumbersome task, an

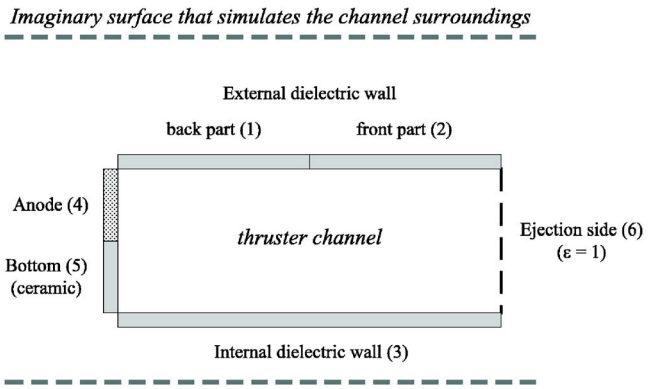

FIG. 3. Radiative enclosure used to solve the energy conservation equation of the thruster channel (shown in cross section for simplicity). The enclosure is divided into six-isothermal surfaces. A virtual surface that surrounds the enclosure simulates the channel environment.

option consists in treating the problem of radiation exchange in a thermal enclosure. The latter will be defined by the channel walls, and the impact of other thruster components (e.g., coils, housing, and cathode) will be simulated by an isothermal surface surrounding the channel, as can be seen in Fig. 3.

1. Assumptions and energy equation

Whatever the approach, a thermal model is naturally based on Eq. (4). In order to derive the appropriate form of the energy conservation equation, the following assumptions are made: heat conduction along the z and θ directions is neglected, the environment is at a low pressure and it exhibits a fixed temperature T_{env}, the atomic plasma is optically thin for thermal radiation wavelengths, the external channel wall radiates part of its energy outward, the internal wall loses no energy through its inner side (adiabatic wall), plasma properties are stationary (q_p does not depend on time), and the thermodynamic parameters do not depend on the temperature. Therefore, the remaining energy rates involved in our study are a conductive heat flux through the channel walls, a radiative flux for all surfaces, the energy deposited by the plasma q_p, which is an unknown variable, and for the outer side of the external dielectric wall, a thermal radiation heat flux toward the outside (ϕ_{outside}). The drawing in Fig. 2 indicates all energy fluxes taken into account in the thermal model.

With these assumptions, the energy conservation equation reduces to the well-known unsteady heat-conduction equation with no sources or sinks,

$$\frac{\partial T(r,t)}{\partial t} = \alpha \frac{\partial^2 T(r,t)}{\partial r^2}. \tag{7}$$

The appropriate boundary conditions depend on both the considered element and surface, as depicted in Fig. 3,

$$\kappa \frac{\partial T}{\partial r}\bigg|_{r=0} = -\phi_{\mathrm{rad}} + q_p \quad \text{for both the internal and external walls,} \tag{8}$$

$$\kappa \frac{\partial T}{\partial r}\bigg|_{r=h} = -\phi_{\mathrm{outside}} \quad \text{for the external wall,} \tag{9}$$

$$=0 \quad \text{for the internal wall,} \tag{10}$$

where κ is the thermal conductivity. At that point a formula is needed to describe ϕ_{rad}, and the reason why the expression "semiempirical model" is employed must be explained.

2. Thermal enclosure and radiative heat flux

The conductive heat flux is obtained by locally applying Fourier's law of heat conduction. In radiation, the problem of heat transfer is far more complex as it is nonlocal leading to heat balances in the form of integral equations.[12] Numerous efforts are devoted to computation of thermal radiation heat transfers using, for instance, ray tracing schemes or statistical methods.[12,13] We propose here a more simple approach by describing the thruster channel as a thermal enclosure and using geometrical factors to compute energy exchanges.[12]

As can be seen in Fig. 3, the channel is considered as an enclosure composed of several surfaces that are individually isothermal. Moreover, it is assumed that within the enclosure energy is emitted diffusely and the incident energy flux is uniform over each individual area. The exact shape and properties of the enclosure are, in fact, directly linked to configuration of the infrared thermal imaging experimental arrangement.[5] Indeed, the angle shot solely permits us to observe five major parts (see Fig. 3): The external wall back (1) and fore (2) parts, the internal wall (3), the anode (4), and the bottom (5). The back part of the internal wall being not accessible with our setup, the entire internal wall surface is assumed to be isothermal. The enclosure is completed with the ejection face (6), which is considered as a blackbody at the uniform temperature T_{env}. Yet, in the case of both the SPT100 and the PPS®1350 thrusters, the channel bottom is not accounted for as the anode covers the whole end side of the channel. Only five areas are then considered.

Radiation exchanges in an enclosure are calculated by means of geometrical configuration (or view) factors F. Such factors define the fraction of heat exchanged between each individual surface.[12] For an enclosure shape as simple as the one we proposed, the view factors can be found in literature.[14] Note that parts 1, 2, and 3 are cylinders and parts 4, 5, and 6 are either ring or disk in view of the cylindrical geometry of the channel (see Fig. 1). Theoretical values of some view factors are given in Table I for the PPSX000-ML thruster.

Within an enclosure, radiative heat flux (in $\mathrm{W/m^2}$) for an element k of area A_k can be written as

$$\phi_{\mathrm{rad}}(z) \approx \sigma\left(\varepsilon_k T_k^4 - \sum_i \varepsilon_i F_{ki} T_i^4\right), \tag{11}$$

where σ is the Stefan-Boltzmann constant, ε is the normal spectral emissivity,[5] T_k is the element surface temperature, T_i is the temperature of the ith surface facing the considered element, and F_{ki} the blackbody configuration factor between the element k and the environment element i.[12] Radiation exchange is considered here within an enclosure composed of gray isothermal surfaces with finite areas neglecting re-

TABLE I. Theoretical blackbody (F_{ki}) and graybody (F_{ki}) configuration factors for the rear part of the external ceramic wall ($k=1$) and the internal ceramic wall ($k=3$) of the PPSX000-ML thruster equipped with a carbon anode. The fitted G factors are obtained from the observed wall temperature temporal evolution after thruster shutoff. Note that G_{k6} factors cannot be experimentally determined.

i index	1	2	3	4	5	6
Theoretical F_{1i}	0.0531	0.0932	0.3924	0.2556	0.1031	0.1026
Theoretical G_{1i}	0.0508	0.0917	0.3706	0.1792	0.1005	0.1017
Fitted G_{1i}	0.09	0.12	0.43	0.36	0.13	…
Theoretical F_{3i}	0.283	0.283	0	0.0876	0.1292	0.2172
Theoretical G_{3i}	0.2673	0.2673	0	0.0731	0.1242	0.2132
Fitted G_{3i}	0.28	0.28	0	0.11	0.12	…

flected energy (ε close to 1). In the RHS of Eq. (11), the first term corresponds to the amount of thermal radiation evacuated by the element surface, whereas the second term corresponds to heat flux received from surrounding surfaces.

To allow in a realistic way for departure from blackbody properties, it is better to use graybody configuration factor G instead of F factors. The radiative heat flux then becomes

$$\phi_{\text{rad}}(z) = \sigma\left(\varepsilon_k T_k^4 - \sum_i \varepsilon_i G_{ki} T_i^4\right). \tag{12}$$

The theoretical expression of G factors will be given in Sec. III. Combining Eqs. (7)–(10) and (12) one notices that to compute the temperature of a given channel wall parts implies to know at each time step the temperature of all other parts as well as the spatial distribution of the energy flux q_p. In other words, bearing in mind that the objective is to assess the value q_p, the determination of the latter necessitates to know about the evolution through time of all channel component temperature fields and vice versa.

3. Adding the measured temperature fields

In order to solve the paradox and to determine q_p, numerical simulations of the thruster channel thermal behavior use, as input data, measured temperature fields. The adjective semiempirical is then well suited as for an enclosure element k at the unknown temperature T_k, the values of other elements' temperature T_i are the ones recorded by means of infrared imaging.[5] Advantages of this semiempirical approach are twofold, namely, it allows us to drastically reduce the number of parameters, as T_k and q_p remain the only variables, and brings closer the simulations to the real thermal behavior of the thruster.

At calculation launch ($t=0$) we assume that the temperature of the walls is equal to the surface's temperatures, which are recorded by infrared imaging. Having a small initial gradient through the wall, however, does not change the results.[10] In Fig. 4, the measured mean temperature of various parts of the PPSX000-ML thruster channel dielectric wall is plotted as a function of time. Such series of temperature profiles are used in the simulations. The experimental setup and thermogram acquisition have been extensively described elsewhere.[5,11] The IR camera is equipped with a GaAs quantum well infrared photodetector (QWIP) that collects thermal radiation in the 8–9 μm domain. A temperature range from −20 to 2000 °C can be probed with a frame rate up to 750 Hz. The latter allows us to perform time-resolved measurement with a good accuracy, as characteristic time scales for both conductive and radiative heat exchanges are longer than 0.1 s under our conditions. For the various materials, the spectral emissivity ε was measured as a function of both the wavelength and the temperature. A statistical analysis reveals that the error in the wall temperature is below ±4%.[5]

All the necessary elements are now available to write down the form of the energy conservation equation, which must be solved for a given enclosure part. For the sake of clarity heat conduction is neglected here. The equation is given for the back part of the external channel wall (see Fig. 3),

$$\rho c_p \frac{dT_1(t)}{dt} h = \sigma\varepsilon_1 T_1(t)^4 (G_{11} - 1 - F_{\text{out}}) + \sigma\varepsilon_2 G_{12} \bar{T}_{12}(t)^4 + \cdots + \sigma\varepsilon_6 G_{16} \bar{T}_{\text{env}}(t)^4 + q_p, \tag{13}$$

where $\bar{T}$ refers to the surface average temperature, which is experimentally determined by infrared imaging, and F_{out} is a view factor that characterizes heat losses toward the outside, as explained in the next section. Even if two variables re-

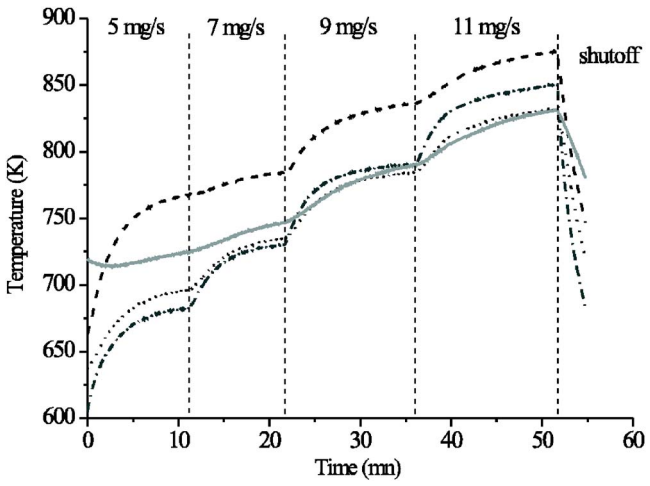

FIG. 4. Evolution through time of the temperature of various parts of the PPSX000-ML thruster channel when varying the gas flow rate (U_d =400 V): back (dot) and fore (dash dot) parts of the external wall, internal wall, (dash) and bottom (solid line). The last sequences correspond to thruster shutoff. Measurements are performed with a calibrated infrared camera (BN–SiO_2 ceramic, ε=0.92) (Ref. 5).

mains, i.e., T_k and q_p, varying q_p in an iterative manner permits us to compute T_k in such a way that a good agreement between numerical profile and measured profile is reached.

The thermal model gives satisfactory results for external and internal wall temperatures. However, it fails in correctly reproducing the anode and bottom temperature profiles. Indeed we do not consider heat exchange between the anode, the ceramic channel bottom, and the thruster rear parts. As a remedy, an adjustable parameter β is introduced into the anode and bottom energy equation to account for outward energy losses. The outward energy flux is written in the form $\phi_{\text{outside}}=\beta_{4,5}\sigma\varepsilon_{4,5}T_{4,5}^4$. Hence, according to Eq. (5), the energy equation without heat conduction reads

$$\rho c_p \frac{dT_{4,5}(t)}{dt} h = -\sigma\varepsilon_{4,5}T_{4,5}(t)^4(1+\beta_{4,5}) + \cdots + q_p. \quad (14)$$

The value of β typically lies in the range (1–1.5). The use of β permits us to obtain proper computed temperature profiles. Yet, it shows the intrinsic limit of our thermal model. It also means that the amount of energy lost by the plasma onto both the anode and the channel bottom cannot so far be determined with a good accuracy.

III. CONFIGURATION FACTORS

A. *G* factor calculation and outward losses

At that point, Eq. (13) cannot yet be solved. Indeed, values of graybody configuration factors G_{ki} have first to be calculated for the chosen enclosure. In contrast to view factors F_{ki}, they do not only depend on the geometry of the surfaces but also on their radiative properties. For two isothermal surfaces S_k and S_i, respectively, at temperatures T_k and T_i, the net radiation exchanged Φ_{ki} between k and i is for a blackbody,

$$\Phi_{ki} = \sigma F_{ki}(T_k^4 - T_i^4)A_k. \quad (15)$$

In a similar manner, for a graybody,[15,16]

$$\Phi_{ki} = \sigma G_{ki}(\varepsilon_k T_k^4 - \varepsilon_i T_i^4)A_k \quad \text{with} \quad G_{ki} = \frac{1}{(1-\varepsilon_k)/\varepsilon_k + 1/F_{ki} + [(1-\varepsilon_i)/\varepsilon_i](A_k/A_i)}. \quad (16)$$

This is the formula we will use in this work to calculate graybody view factors of the enclosure elements. Computed values of some G_{ki} factors are given in Table I for the PPSX000-ML thruster.

There is a last factor which must be determined: The heat flux radiated outward by the external dielectric wall through its outer surface. The external wall is surrounded by thruster elements such as coils and magnetic circuit pieces as well as the vacuum vessel. A full modeling of heat exchange between the external wall and its vicinity is far too complex. Instead, the environment of the external wall is simulated by a virtual surface located at $\frac{1}{2}r_{\text{ext}}$ from the external ring, where r_{ext} is the external wall radius. The length of this imaginary surface is twice the length of the channel. As can be seen in Fig. 3, this virtual cylinder solely extends beyond the end (bottom) of the channel. The temperature T_{env} of the virtual cylinder is kept constant at 450 K, in agreement with temperature measured by thermocouples embedded in the thruster structure for moderate applied power (~2 kW). The net radiation exchange Φ_{outside} between the outer surface of the external wall and its virtual environment can be treated as heat exchange between two bodies at uniform temperature,

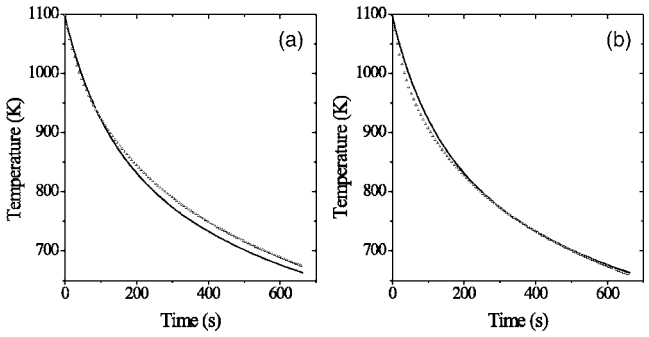

FIG. 5. Mean temperature of the internal channel wall as a function of time after shutoff of the PPSX000-ML thruster. (a) Comparison between experimental data (solid line) and numerical outcomes (triangle) using theoretical graybody view factors G. (b) The computed curve is fitted to the measured profile by changing G factor values. The obtained set of fitted G factors is then used to carry out thruster thermal behavior simulations.

$$\Phi_{\text{outside}} \approx \sigma F_{\text{out}}(\varepsilon T_{1,2}^4 - T_{\text{env}}^4)A_{1,2} \approx \sigma\varepsilon F_{\text{out}}T_{1,2}^4 A_{1,2}, \quad (17)$$

where F_{out} is the view factor between the external wall and the virtual cylinder and A the area of the outer side of the channel external wall. As $T_{\text{env}} \ll T_{1,2}$, the amount of heat generated by the virtual surface is neglected, the latter being then seen as a heat sink. The F_{out} factor can be calculated theoretically:[14] one finds $F_{\text{out}}=0.6$ for the PPSX000-ML thruster.[14] To include the impact of the thruster environment in the thermal model, the F_{out} factor must be added to G_{11} or G_{22}, as shown in Eq. (13). Outward losses are also taken into account for the anode and the channel bottom, however, in an indirect manner, as shown in Eq. (14).

With such complicated boundary conditions and geometry, Eq. (7) cannot be solved analytically and one must turn toward a numerical approach. We used a finite element method, each part of the channel wall being divided into ten cells with a dimension $\Delta r=h/10$.[10] The time step is around 10^{-2} s to warrant convergence.

B. Fitting the configuration factors

Model outcomes must now be compared with thermal imaging recordings to check the validity of all assumptions as well as to verify whether the geometry of the thermal enclosure permits us to stick to reality. In order to cancel out the impact of the plasma, the comparison must be carried out with a data set collected after a power shutdown, in such a way that q_p vanishes into equations. The result of the comparison can be seen in Fig. 5(a) for the PPSX000-ML thruster. The graph shows that the simulation mimics the measured temperature drop with a good accuracy. The slight temperature difference is mostly due to the fact that nearby heat sources or sinks, e.g., coils and magnetic circuit elements, are not considered in the thermal model.

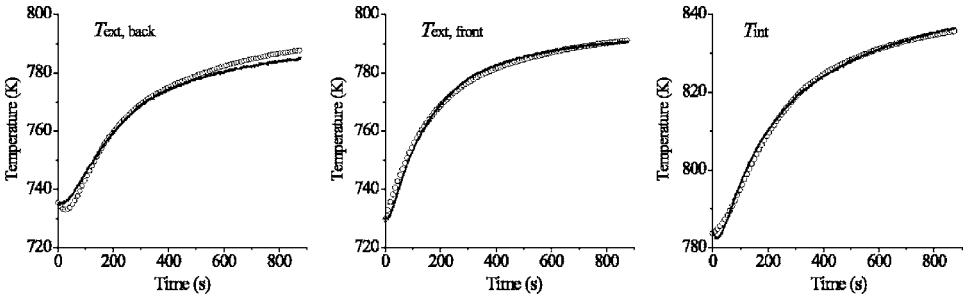

FIG. 6. Evolution in time of the channel wall temperature for a PPSX000-ML thruster operating at 3.3 kW (400 V and 9 mg/s): thermal imaging data (line) and numerical outcome using fitted G factors (circle). From left to right: back and front sections of the external dielectric wall and internal dielectric wall. The corresponding values of q_p are 0.1, 1.4, and 0.5 W/cm^2, respectively.

One way to get closer to the real HET thermal behavior is to subtly modify the value of G factors to account for additional heat exchanges. The method is the following, data sets recorded after thruster shutdown are used to fit G factors in such a way that measured and calculated temperature profiles do match each other. Figure 5(b) shows an example of fitting procedure outcome. To calculate G_{ki}, the average temperature $\bar{T}_i$ of the surface i is used. As can be verified in Table I, the gap between theoretical and fitted G factors is rather low but for G_{k4} due to the introduction of the parameter β. Furthermore, for a given thruster configuration, the G factor values do not differ when using several data sets. Note that G_{k6} factors cannot be experimentally determined; however, the ejection side plays a minor role in view of its low temperature.

IV. POWER LOSSES ON THE THRUSTER CHANNEL WALLS

A. Extraction of q_p

The time-dependent semiempirical thermal model, based on measured temperature fields and experimental view factors, is then used to assess the energy flux or power per unit area q_p delivered by the plasma to the inner and outer walls of the thruster channel. The quantity, which is the only unknown parameter in the model, is obtained by adjusting in an iterative manner the calculated temperature profile to the one measured by means of calibrated infrared imaging until a satisfactory agreement is reached. An example of data extraction process is shown in Fig. 6 for the PPSX000-ML thruster operating at 3.3 kW input power. As can be seen, the calculated mean temperature curve matches up the measured curve for the three BN–SiO_2 channel wall parts. In the range of input electrical power covered in this work, i.e., 500–5000 W, typical values for q_p lie in the range of 0.1–2 W/cm^2, whatever the thruster.

A sensitivity analysis was carried out in order to estimate the error bar magnitude for the q_p quantity.[10] The impact of wall temperatures and view factors upon q_p was investigated using the thermal model. For several operating conditions of the PPSX000-ML thruster the temperature of enclosure elements was changed by ±50 K keeping G factors fixed. In a similar manner, G factors were simultaneously or alternately changed by ±20% keeping the temperature unchanged. Combining all results, the uncertainty introduced by the semiempirical approach was estimated as ±25% at maximum for the experimental value of q_p. Note that energy losses onto the anode and/or the channel bottom are not reported here, as discussed in Sec. II C 3.

B. Evolution of q_p with applied voltage and input power

In Fig. 7 the amount of power lost per unit area q_p is plotted as a function of the applied voltage for three channel wall parts of the PPSX000-ML thruster. The latter was magnetically optimized during the measurement series. First, q_p depends strongly on the applied voltage U_d. Second, most of the power is delivered to the front part of the external dielectric wall, whatever the propellant mass flow rate, as can clearly be seen in Fig. 7. These two points are in favor of an energy deposition mechanism dominated by ion impact onto the final section of the wall.[5,17] Ions are strongly accelerated at the channel outlet where the axial electric field is high.[18] Moreover, the ion velocity magnitude is related to U_d.[18] As shown in Fig. 7, the quantity q_p also increases with the injected xenon mass flow rate due to an increase in the amount of ions produced inside the channel.

Another way to present the obtained data is to plot q_p as a function of the input electrical power $P=U_d \times I_d$, where I_d is the discharge current. The resulting graph is shown in Fig. 8. The trend is naturally similar to the one observed previ-

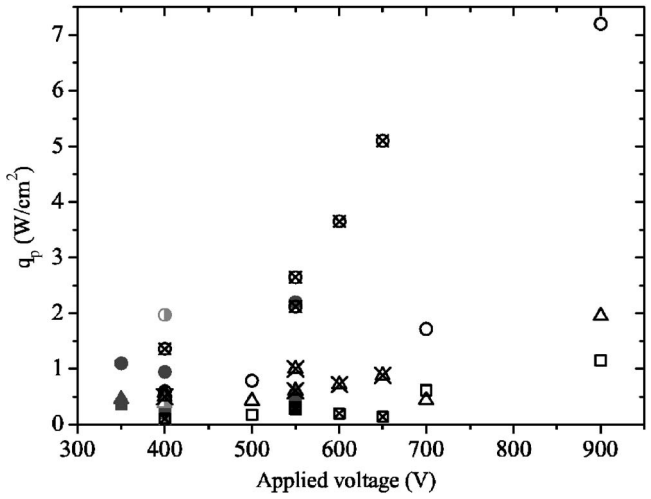

FIG. 7. Amount of power per unit area q_p delivered by the plasma onto the channel dielectric wall of the PSSX000-ML thruster as a function of the applied voltage: back (square) and front (circle) sections of the external wall and internal wall (triangle). The propellant mass flow rates were changed: 4–5 mg/s (open symbols), 6–7 mg/s (full symbols), 7.5–9 mg/s (symbols with a cross), and 11 mg/s (half filled symbols).

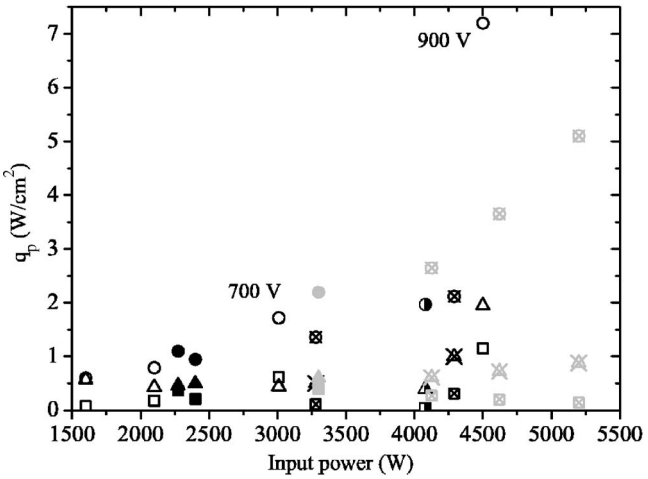

FIG. 8. Q_p vs input electrical power for the PPSX000-ML thruster: back (square) and front (circle) sections of the external wall and internal wall (triangle). The propellant mass flow rates were varied: 4–5 mg/s (open symbols), 6–7 mg/s (full symbols), 7.5–9 mg/s (symbols with a cross), and 11 mg/s (half filled symbols). Black symbols are for a carbon anode and gray symbols are for a stainless steel anode.

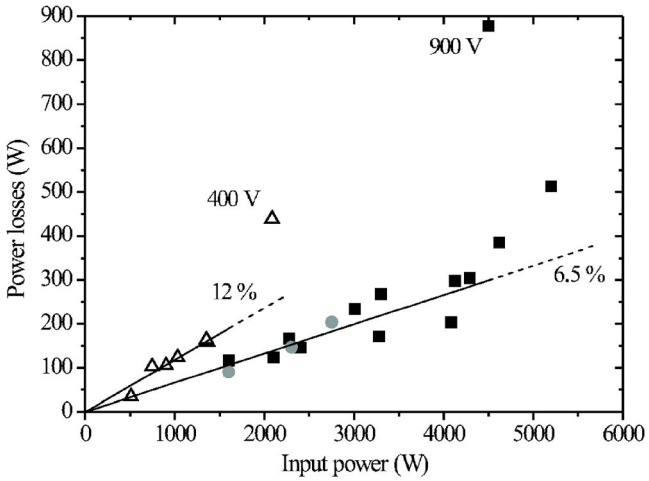

FIG. 9. Power losses on $BN-SiO_2$ channel walls as a function of the input electrical power: PPSX000-ML (square), PPS®1350 (circle), and SPT100-ML (triangle). Lines are linear fits to SPT100 and PPSX000-ML datasets.

ously. The amount of power delivered to the dielectric wall increases with the input power. Losses occur mostly in the far end of the channel. The graph also shows that for a fixed input power, seeded mass flow rate and applied voltage do not have the same impact on q_p. Power losses are mainly driven by applied voltage. In Figs. 7 and 8 the evolution of q_p changes suddenly when U_d is above ≈600 V. The large value of q_p in the high discharge voltage domain could be explained by the production of multiply charged ion species. Several works have shown that the creation of multiply charged ions inside the thruster channel, especially Xe^{2+} and Xe^{3+} ions, is favored at high voltage.[19–22] For instance, measurements carried out by means of an $\mathbf{E}\times\mathbf{B}$ probe in the plasma plume of a 5-kW-class NASA-173Mv2 thruster indicate that the on-axis Xe^{2+} and Xe^{3+} ion fractions are 0.12 and 0.02, respectively, at 900 V for a 10 mg/s gas flow.[21] Traces of Xe^{4+} ions have also been detected.[20] As ion kinetic energy is proportional to the electric charge, production of multiply charged ions contributes to increasing the amount of energy delivered to the channel walls. In other words, thermal losses of a multiply charged ion beam are larger than that of a singly charged ion beam. In addition to reducing the thrust efficiency, production of multiply charged ions is responsible for thruster lifetime decrease as wall sputtering is favored at high ion energy. Other mechanisms could yet be at the origin of the observed drastic increase of q_p when a thruster is operated at high voltage. For instance a change of the plasma sheath properties at high electron energy could cause the ion current losses onto walls to increase.[23] It may then be necessary to adapt the magnetic field topology for high voltage operations in order to limit plasma-wall interactions.[24] Note that the anode material does not play any role in the value of q_p, as the anode was either made out of stainless steel or made out of carbon (see Fig. 8).

C. Influence of thruster design

Instead of studying power losses per unit area, another approach consists in examining power losses on the entire channel wall area. The total power delivered to external and internal discharge chamber walls P_{wall} is computed as follows:

$$P_{\text{wall}} = \frac{1}{2}A_{\text{ext}} \times (q_{p,1} + q_{p,2}) + A_{\text{int}} \times q_{p,3}, \tag{18}$$

where A refers to area. The calculation is dictated by the thermal enclosure geometry (see Fig. 3).

In Fig. 9, the amount of power passed to the dielectric $BN-SiO_2$ channel walls is plotted as a function of the input electrical power P for the PPSX000-ML, PPS®1350-G, and SPT100-ML thrusters. All points are magnetically optimized to minimize discharge current. First, P_{wall} varies linearly with the applied power as long as voltage and gas flow are not well above standard values. Second, P_{wall} is solely a small fraction of the applied power, whatever the thruster: $P_{\text{wall}} \approx 6.5\%$, 7%, and 12% of the input power for the PPSX000-ML, PPS®1350-G, and SPT100-ML thrusters, respectively. In a recent work, Kim *et al.* estimated the amount of energy released by the plasma at the channel wall of a PPS®1350 Hall thruster operating in a high specific impulse domain.[17] They used a method very similar to the one described in Sec. II B, as it is based on temperature changes due to power interruption. They found power losses of 205 W at 1500 W input power (350 V and 4.28 A), which means about 14%. Accounting for a ±25% uncertainty for the value of q_p, one finds $P_{\text{wall}} = 91 \pm 23$ W at 1600 W applied electrical power in this work. The agreement between outcomes of the Russian study and results shown in Fig. 9 is poor; however, several remarks are worth making. The result of Kim *et al.* relies on measured dielectric wall thermal capacity. They used only two thermocouples embedded in the dielectric walls. Their technique suffers from a low accuracy level such as the go and stop approach described in this contribution. On the contrary, the value of power losses obtained with the semiempirical time-dependent thermal model is identical to the one estimated from electron properties and ion current measurements.[5,17] In the case of a PPS®1350

thruster operating at 1350 W the thermal model gives 56 W and plasma parameter measurements yield 60 W for the final section of the external wall.

A linear law for the evolution of P_{wall} with P is not really a surprise. A first-order approximation, i.e., a picture in which only one type of ions is considered and in which the electron contribution as well as plasma sheath formation is neglected, indicates that the amount of power passed to the channel walls depends on both the ion kinetic energy and the ion current to the walls.[5] The former is roughly proportional to the discharge voltage U_d, and the latter can be expressed as a fraction of the discharge current I_d. Hence, P_{wall} varies as $U_d \times I_d$. The real behavior is, in fact, more complex as one must account for sheath formation in a magnetized plasma, ion internal energy, production of multiply charged ions, electron current to the wall, secondary electron emission, and wall erosion. Nevertheless, experimental data reveal that a picture solely based on Xe^+ ion bombardment is valid for reasonable input power levels. At high input power, departure from the initial trend is expected in view of the abundant production of multiply charged ion species. For the PPSX000-ML, above 4.5 kW P_{wall} is in excess of 6.5% of the input power, as shown in Fig. 9. It reaches up to 19.5% when the thruster is operated at 900 V discharge voltage. In the case of the SPT100-ML thruster, P_{wall} is found to reach 21% of the input power at 2100 W.

As can be seen in Fig. 9, power losses are much less for the PPS®1350-G in comparison with the SPT100-ML, whereas the two thrusters exhibit almost identical dimensions. The optimized magnetic field line topology of the former limits plasma-surface interactions while allowing to reach a high efficiency. Furthermore, the good thermal design of the PPS®1350-G thruster allows operation at high power, as it was fired up to 3200 W without suffering from the heat load.[25] At a given input power, losses at walls are almost identical for the PPSX000-ML and the PPS®1350-G thrusters. However, the energy flux q_p is higher for the PPS®1350-G by about a factor of 2. It explains the higher steady state wall temperature in the case of the PPS®1350-G thruster.[5] The thermal design of the PPSX000-ML enables operation at power above 5 kW despite the high value of P_{wall}. Radiators have an optimized architecture. The thruster body and magnetic circuit are open to enable the external dielectric wall to evacuate most of its thermal power outward without heating too much its surroundings. In such a way the amount of power stored in secondary heat sources such as metal elements and coils is limited. Note that the small surface to volume ratio of the PPSX000-ML restricts energy losses through walls.

A last point must be outlined. The amount of power passed to Hall thruster dielectric channel walls is between 5% and 15% of the applied power. Neglecting losses at the channel bottom, the overall power losses inside the channel are obtained by accounting for the amount of power lost by electrons at the anode P_{anode}. Such a term can be written as $P_{\text{anode}}=I_d \times \frac{5}{2}\hat{T}_e$, where $\hat{T}_e$ is the electron temperature in eV in the anode vicinity.[5] P_{anode} typically represents less than 10% of the applied electrical power since under standard conditions $\hat{T}_e$ is less than 15 eV.[26] Therefore the overall power losses in the channel are below 25% of the applied power. The thrust efficiency of modern Hall effect thrusters is around 60% over a broad range of power. Hence, plasma-wall interactions inside the channel cannot explain the efficiency level even when accounting for ionization losses. Other loss mechanisms must then be put forwards such as beam divergence, scattering in ion kinetic energy, and energy dissipation owing to transport of electron through the magnetic barrier.

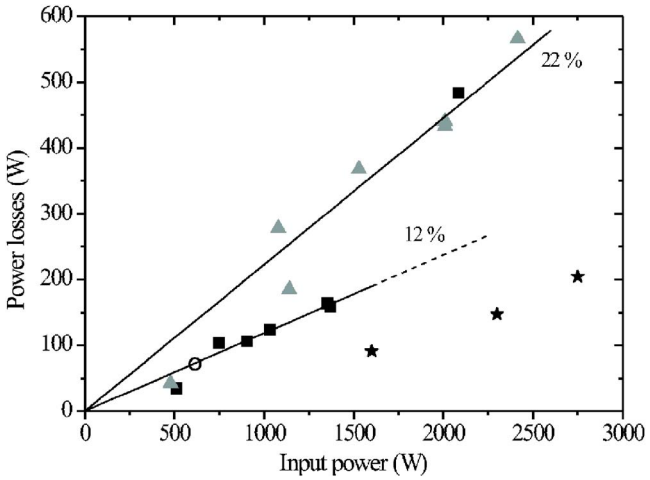

FIG. 10. Power losses on SPT100-ML thruster channel walls for various materials: $BN-SiO_2$ (square), AlN (triangle), and graphite (circle). Also shown are power losses for the PPS®1350 thruster equipped with $BN-SiO_2$ walls (star).

D. Wall material effect

Figure 10 displays the power losses on STP100-ML walls as a function of the applied electrical power for various materials: $BN-SiO_2$, AlN, and graphite. As a matter of fact, results shown in Fig. 10 indicate that the material has a strong impact on P_{wall}. It is in good agreement with previous studies in which it was shown that the wall material deeply influences the steady state channel temperature.[5] Naturally, material properties such as electric conductivity, secondary electron yield, as well as sputtering rate determine plasma sheath properties, which in turn influence discharge behavior and subsequently the current level.[5,27] It was, for instance, shown that for a given seeded xenon mass flow rate the discharge current is higher when AlN is used.[5,27] As a consequence, the ion flux to the walls is higher due to either a larger number of ions directly impinging onto walls or a larger electron current to the walls. In both cases plasma-surface interactions are more important when AlN is employed, as can be seen in Fig. 10. Also visible in this figure is the fact that the P_{wall} is a linear function of P, whatever the material. P_{wall} reaches 22% of the input power with AlN, whereas it is only 12% with $BN-SiO_2$.

V. CONCLUSION

The approach described in this article is promising for both engineers and scientists as it allows us to assess with a reasonable accuracy the power per unit area q_p, as well as the

total power, delivered by the plasma to HET channel walls. In spite of a relative lack of spatial resolution, as the discharge chamber can solely be divided into a few elementary surfaces to warrant small error bars for q_p, and notwithstanding the fact that heat exchanges between the channel and its direct surrounding are treated in a simple manner, this method furnishes valuable data in terms of energy flux that can be compared to outcomes of hybrid Hall thruster model.

A primary challenge in the comparison between numerical simulations and experimental data is the understanding of mechanisms responsible for energy transfer to channel walls. This work tends to demonstrate that energy losses are mostly due to ion bombardment. However, the role of electrons must be clarified as hot electrons could deliver a non-negligible amount of energy. Furthermore, interaction between electrons and walls upstream of the channel exit plane could explain the relatively low electron temperature measured in the core of the plasma. In a similar manner the role of UV radiations has to be investigated. A second aspect applies to plasma sheath. Experimental values of q_p can naturally be used to refine modeling of plasma sheath. Indeed, the fraction of input power transfer to walls strongly depends on sheath properties at dielectric channel walls. Additionally, the study on plasma-surface interactions inside a HET gives useful information about the plasma properties. Present results show that multiply charged ion species are produced under high voltage and that they collide with walls, which leads to a drastic increase in power losses. Such a phenomenon must of course be reproduced by hybrid models.

ACKNOWLEDGMENTS

The authors greatly appreciate fruitful discussions with Professor M. Dudeck and Dr. P. Echegut. They are indebted to Dr. E. Barbosa for his critical review of the preliminary version of this article. This work is carried out in the frame of the joint research program CNRS/CNES/Snecma/Universités 2759 "Propulsion Spatiale à Plasma."

[1]M. Martinez-Sanchez and J. E. Pollard, J. Propul. Power **14**, 688 (1998).
[2]R. H. Frisbee, J. Propul. Power **19**, 1129 (2003).
[3]V. V. Zhurin, H. R. Kaufman, and R. S. Robinson, Plasma Sources Sci. Technol. **8**, R1 (1999).
[4]V. Kim, V. Kozlov, G. Popov, A. I. Skrylnikov, K. Kozubsky, and M. Lyszyk, Proceedings of the 26th International Electric Propulsion Conference (IEPC), Kitakyushu, Japan, 1999, Paper No. 84.
[5]S. Mazouffre, P. Echegut, and M. Dudeck, Plasma Sources Sci. Technol. **16**, 13 (2006).
[6]S. Mazouffre, F. Dubois, M. Dudeck, and P. Echegut, Proceedings of the Fourth International Spacecraft Propulsion Conference, Sardina, Italy, 2004.
[7]V. Kim, J. Propul. Power **14**, 736 (1998).
[8]J. F. Sacadura, *Initiation aux Transferts Thermiques*, 4th ed. (Technique et Documentation, Paris, 1993) (in French).
[9]M. Jakob, *Heat Transfer*, 6th ed. (Wiley, New York, 1958), Vol. 1.
[10]J. Pérez-Luna, Laboratoire d'Aérothermique Internal Report No. RS 2005-08, 2005 (unpublished).
[11]S. Mazouffre, J. Pérez-Luna, D. Gawron, M. Dudeck, and P. Echegut, Proceedings of the 29th International Electric Propulsion Conference, Princeton University, NJ, 2005, Paper No. 63. The reader may point out that another formula is employed in this article to express the radiative heat flux. The two formulas are fully equivalent in the case of blackbodies ($\varepsilon=1$), thanks to the configuration factor reciprocity principle (Ref. 12). The use of an alternative form for ϕ_{rad} in this contribution leads to slightly different values of q_p.
[12]R. Siegel and J. R. Howel, *Thermal Radiation Heat Transfer* (McGraw-Hill, New York, 1972).
[13]J. R. Mahan, *Radiation Heat Transfer: A Statistical Approach* (Wiley, New York, 2002).
[14]J. R. Howell, A Catalog Radiation Heat Transfer Configuration Factors (http://www.me.utexas.edu/howell/) and references herein.
[15]F. Kreith, *Principles of Heat Transfer*, 2nd ed. (International Textbook, Scrantom, 1965).
[16]F. R. G. Eckert and R. M. Drake Jr., *Heat and Mass Transfer*, 2nd ed. (McGraw-Hill, New York, 1959).
[17]V. Kim, V. Kozlov, A. I. Skrylnikov, L. N. Umnitsin, V. V. Svotina, A. Bouchoule, and M. Prioul, Proceedings of the 29th International Electric Propulsion Conference (IEPC), Princeton University, NJ, 2005, Paper No. 4.
[18]D. Gawron, S. Mazouffre, L. Albarède, and N. Sadeghi, Proceedings of the 42nd AIAA/ASME/SAE/ASEE Joint Propulsion Conference (AIAA), Sacramento, California, 2006, Paper No. 06-4473, and references herein.
[19]A. Lazurenko, V. Vial, A. Bouchoule, A. Skrylnikov, V. Kozlov, and V. Kim, J. Propul. Power **22**, 38 (2006).
[20]F. S. Gulczinski and A. D. Gallimore, J. Propul. Power **17**, 418 (2001).
[21]R. R. Hofer and A. D. Gallimore, Proceedings of the 39th AIAA/ASME/SAE/ASEE Joint Propulsion Conference (AIAA), Huntsville, Alabama, 2003, Paper No. 03-5001.
[22]R. R. Hofer and A. D. Gallimore, J. Propul. Power **22**, 732 (2006).
[23]Y. Raitses, D. Staack, M. Keidar, and N. J. Fisch, Phys. Plasmas **12**, 057104 (2005).
[24]S. Mazouffre, A. Lazurenko, P. Lasgorceix, M. Dudeck, S. d'Escrivan, and O. Duchemin, Proceedings of the Seventh International Symposium on Launcher Technologies, Barcelona, Spain, 2007, Paper No. O-25.
[25]V. Vial, A. Lazurenko, M. Prioul, L. Garrigues, A. Bouchoule, and J. Boeuf, Proceedings of the 40th AIAA/ASME/SAE/ASEE Joint Propulsion Conference (AIAA), Fort Lauderdale, Florida, 2004, Paper No. 04-3607.
[26]J. A. Linnel and A. D. Gallimore, Phys. Plasmas **13**, 103504 (2006).
[27]N. Gascon, M. Dudeck, and S. Barral, Phys. Plasmas **10**, 4123 (2003).